PLOS Climate

RESEARCH ARTICLE

The inflationary effects of the El Niño-Southern Oscillation

Marco Gallegati[1], **Solomos Solomou**[2*], **Kun Tian**[3]

1 DISES, Polytechnic University of Marche, Ancona, Italy, **2** Faculty of Economics, University of Cambridge, Cambridge, United Kingdom, **3** Kent Business School, University of Kent, Canterbury, United Kingdom

* ss19@cam.ac.uk

Abstract

In this paper we apply the wavelet approach and the GVAR methodology to investigate the effects of El Niño fluctuations on national inflation rates, global commodity prices and world oil prices. The focus of our analysis is on the inflation effects of "ENSO diversity", measured as the central Pacific (CP) and eastern Pacific (EP) El Niño. Using quarterly data from c.1950 onward, we substantially extend the time span of existing studies. This allows us to observe a much larger number of ENSO cycles. The set of countries included in our study comprises countries directly affected by the El Niño, countries that are teleconnected with the El Niño variations and countries that are only indirectly affected by these processes via global economic linkages. The results from wavelet analysis display several key features. First, we observe an episodic relationship between ENSO variations and inflation for most countries, irrespective of whether they are directly impacted by ENSO or impacted via teleconnections. Second, the identification of CP and EP ENSO effects highlights the importance of ENSO diversity when analysing the inflationary effects of ENSO. Third, the periods of statistical significance encompass both El Niño and La Niña phases of the ENSO cycle. The GVAR framework used to estimate the magnitude of the effects of the ENSO cycle on national CPI inflation confirms that modelling the effects of ENSO diversity as captured by CP and EP ENSO measures matters for the identification of their complex nonlinear effects on national inflation rates.

OPEN ACCESS

Citation: Gallegati M, Solomou S, Tian K (2026) The inflationary effects of the El Niño-Southern Oscillation. PLOS Clim 5(8): e0000985. https://doi.org/10.1371/journal.pclm.0000985

Editor: Juan A. Añel, Universidade de Vigo, SPAIN

Received: July 22, 2025

Accepted: June 16, 2026

Published: August 5, 2026

Data availability statement: Data available at https://zenodo.org/records/20344538.

Funding: This work was supported by the University of Cambridge Keynes Fund (grant number JHWZ to SS) and the Cambridge Humanities Research Grants Scheme (no grant number; to SS). The funders had no role in study design, data collection and analysis,

1. Introduction

The El Niño-Southern Oscillation (ENSO) is one of the most prominent fluctuations in the global climate system, with far-reaching economic impacts. A key question in climate economics and in Central Bank policy analysis is whether ENSO affects national inflation rates. The existing literature offers mixed evidence. For instance, [1] finds that El Niño variations account for 10–20% of inflation movements in G7 countries between 1963 and 1998. In contrast, [2], examining CPI inflation across

decision to publish, or preparation of the manuscript.

Competing interests: The authors have declared that no competing interests exist.

22 countries from 1950 to 2000, report a lack of statistically significant correlation between the Southern Oscillation Index (SOI) and national inflation rates.

More recent studies have adopted advanced econometric frameworks to revisit this relationship. Statistically significant inflationary pressures have been identified in countries strongly teleconnected to El Niño events and, more broadly, in the world economy due to pressures that are primarily attributed to increases in both oil and non-oil global commodity prices using the Global Vector Autoregression (GVAR) methodology [3]. They identify the El Niño phase of the ENSO cycle as generating inflationary effects. [4] use a GVAR model with local projections to analyse the effects of the ENSO cycle on inflation, constructing a weighted average of CPI inflation across 20 economies/regions (treating the Euro area as a single entity). The effect of an El Niño shock on inflation is found to be statistically significant in the second half of the year of the shock, with the magnitude of the effect ranging between 0.2 to 0.4 per cent. The La Niña state of the ENSO cycle is also found to be inflationary with a more immediate effect being identified. They find that La Niña events have larger inflation effects than El Niño shocks. Using a local projection panel model to estimate an ENSO-augmented Phillips curve, [5] finds state-dependent inflation dynamics driven by the asymmetric macroeconomic effects of the two ENSO phases. The asymmetry arises along two dimensions by affecting the steepness of the Phillips Curve, with inflation responding more strongly to unemployment gaps during La Niña episodes, and in the direct inflationary effects of ENSO, as La Niña episodes exert stronger and more persistent upward pressure than El Niño events.

A common feature across these quantitative studies is the use of a unique fixed region to represent the ENSO cycle — typically through the Niño 3.4 index or various measures of the Southern Oscillation Index (SOI). A critical dimension in understanding ENSO's economic effects is in recognizing the importance of "ENSO diversity" [6,7]. ENSO diversity is commonly described through two distinct regimes: Eastern Pacific (EP) and Central Pacific (CP) ENSO events. These regimes differ in their spatial structure, intensity, and temporal evolution [8–10]. The EP ENSO events typically exhibit stronger warm sea surface temperature (SST) anomalies, while CP ENSO events display more pronounced cold anomalies [10]. Another notable feature is that recent decades have seen a temporal shift in the location of maximum SST anomalies from the eastern to the central Pacific [11,12], with [8] observing an increased frequency of Central Pacific El Niño episodes. These different ENSO types also generate different climate teleconnections. The observed effects of ENSO diversity on climate teleconnections are summarized in [13]; for example, whilst EP ENSO is associated with heavy rain in Western Latin America, CP ENSO shifts this impact away from Latin America.

In economic analysis, ENSO shocks can be treated as supply-side shocks that can have effects on agricultural yields and prices [14–18], energy demand and energy supply [19,20], global commodity prices [1,21,22] and civil conflicts [23–25]. At a macroeconomic level we may also observe effects on aggregate output [3,26], inflation expectations [27] and effects on commodity futures prices [28,29] that will have feedback loops in the macroeconomic system. Our focus is on the ENSO-inflation nexus within a macroeconomic framework. We recognise that significant research has contributed to understanding the effects of ENSO at a more disaggregated level, focusing on particular sectors and commodities [21]. Within a macroeconomic framework, these sectoral and commodity-specific shocks manifest as national inflationary pressures and effects on global commodity prices. Our macro framework explicitly models how these national effects and global commodity price effects interact in a global system.

The key contribution of our paper is to evaluate the importance of ENSO diversity on inflation at the country level and on global commodity prices. For this purpose, we explore the effects of the variation in the two types of ENSO events prevailing in the Pacific on national inflation rates for a large number of countries over the postwar period. To model the inflationary impacts of ENSO, two key dimensions must be considered: temporal heterogeneity and national heterogeneity, reflecting both time variation in ENSO dynamics and differences in countries' sectoral exposure to climate shocks. To capture these aspects, we apply wavelet-based techniques at the country level and a multivariate GVAR framework to model cross-country linkages and global spillovers. Given the cyclical nature of ENSO, typically occurring over 2–7 year intervals [30,31], wavelet analysis is particularly well-suited for uncovering the evolving nonlinear time-frequency relationships between ENSO variability and inflation. The GVAR methodology complements this approach by modelling the transmission of global shocks — such as CP and EP ENSO events — through interconnected national economies and global spillovers.

Our wavelet-based findings reveal that the inflationary effects of ENSO are episodic and highly heterogeneous across countries. This pattern appears both in countries directly influenced by ENSO and in those affected indirectly through climate teleconnections, with their significance not confined to the major El Niño episodes. The only exception to this heterogeneous pattern is provided by the CP ENSO events since c.2000, for which there is widespread evidence of statistically significant effects on national inflation rates at the 2–4 years frequency band. This finding occurs in coincidence with the time-frequency region where highly significant power is observed for the CP ENSO.

Complementing these findings, the GVAR framework — used to estimate the magnitude of ENSO's effects on national CPI inflation — confirms that explicitly modelling ENSO diversity is important for accurately identifying the complex transmission mechanisms of ENSO shocks across national economies. To capture these dynamics, our empirical strategy employs the GVAR framework to trace the global spillovers arising from domestic inflation responses and ENSO-induced movements in world commodity prices. In this respect, our approach is both complementary to, and distinct from, more disaggregated studies, as it emphasises systemic interactions and cross-border transmission mechanisms.

The rich set of results, along with the number of sensitivity tests, points to the usefulness of separating the CP and EP ENSO processes for the identification of the effects of ENSO cycles on national economies. Our findings show that incorporating this diversity into the analysis provides clearer insight into how different ENSO types affect national inflation and helps reconcile the mixed results reported in previous studies.

The remainder of the paper is structured as follows: Sections 2 and 3 use wavelet-based tools to investigate the characteristic features of EP and CP ENSO indices and to analyse their timescale relationships with country-level inflation. Section 4 integrates wavelet analysis into a GVAR framework to evaluate the multivariate effects of the ENSO cycle. Section 5 concludes with a discussion and summary of key findings.

2. Timescale properties of the EP and CP ENSO

To better understand the complex nonlinear pattern of ENSO events, researchers have introduced different indices constructed from SST anomalies to consider "ENSO diversity" [32]. At least two different types of anomaly centres have been identified, the eastern Pacific (EP) and the central Pacific (CP), which exhibit distinct SST anomaly patterns. [11] suggest the CP ENSO arises from atmospheric forcing rather than the thermocline variation underlying the EP ENSO, reflecting the spatial asymmetry between the strong warm and cold phases of ENSO [6,33]. The EP ENSO has its subsurface anomalies located in the eastern equatorial Pacific (by the coast of South America), whilst the CP ENSO anomalies are located in the central Pacific. The EP ENSO tends to appear more often as strong El Niño events than as strong La Niña events. By contrast, moderate to strong La Niña reflects more onto the CP ENSO pattern. Therefore, EP and CP ENSO modes represent the diversity of ENSO amplitude, as well as the asymmetry in the pattern of El Niño and La Niña [11,34,35].

The CP and EP indices used in this study are based on the dataset developed by [11] and extended by [36]; the data are derived using the regression-empirical orthogonal function (EOF) analysis applied to sea surface temperature anomalies. In Fig 1 we present, in the upper panels, the time-series pattern of the EP (left) and CP (right) ENSO — measured at quarterly frequency between 1950:Q1–2019:Q4 by aggregating monthly data — and, in the lower panels, their probability density functions. The differences in the pattern of the two series in terms of amplitude, duration and symmetry of SST anomalies are clearly visible. The amplitude of ENSO's warm and cold events differs between EP and CP events. The larger positive SST anomalies, such as the El Niño events of 1982–1983 and 1997–1998, are classified as EP El Niños. By contrast, CP events are typically characterized by weaker, moderate SST anomalies. The duration also differs, as EP anomalies are generally shorter, more intense events, compared to longer, more persistent but moderate CP events.

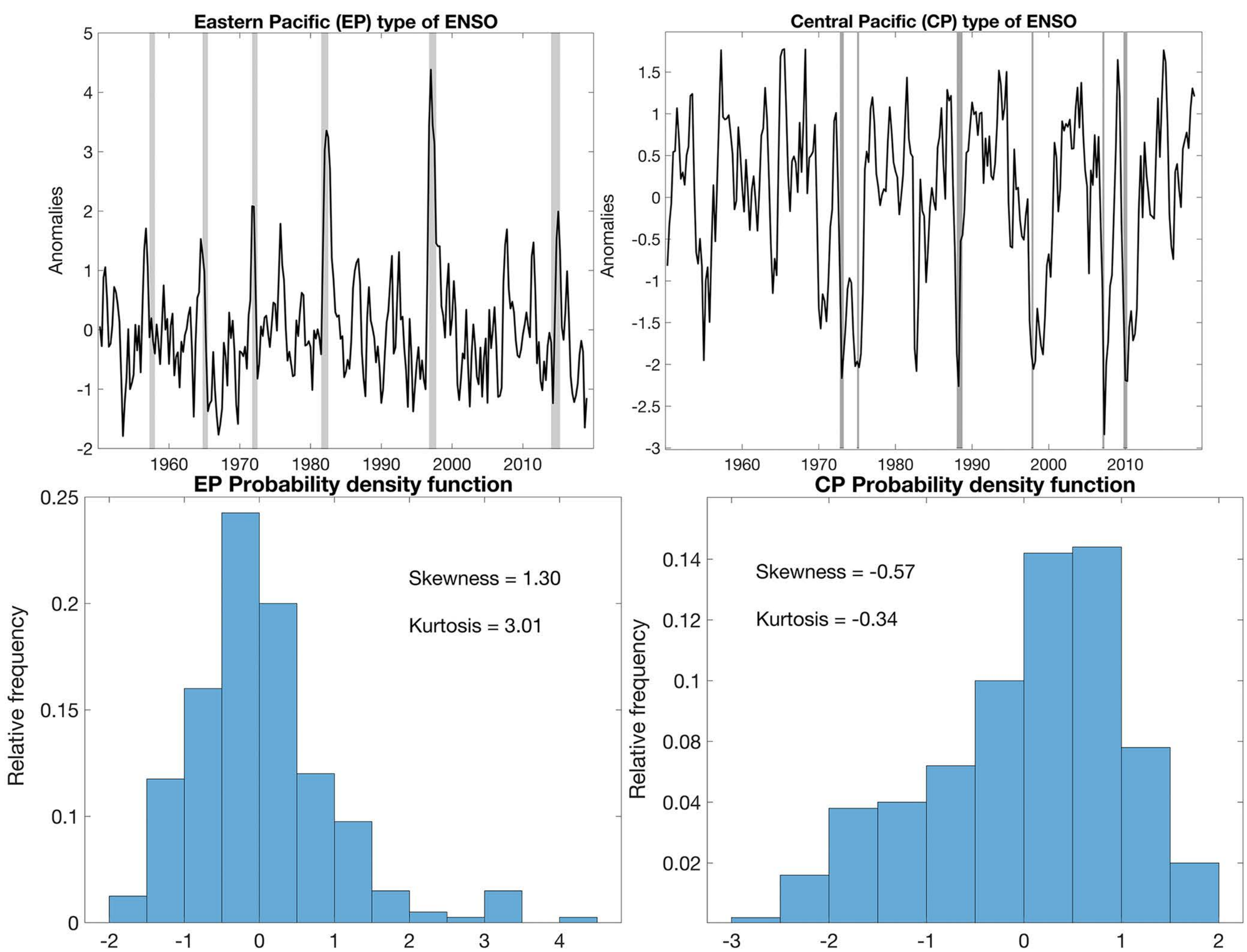

Fig 1. EP (left) and CP (right) types of ENSO (top panels) and their probability density functions (bottom panels). *Note: Grey shaded areas denote strong El Niño and La Niña events in top left and top right panels, respectively.*

https://doi.org/10.1371/journal.pclm.0000985.g001

The asymmetry between EP and CP events is evident in the probability density function (PDF) presented in the lower left and right panels of Fig 1. The values of the skewness and kurtosis coefficients reported within the PDF plots suggest a near Gaussian distribution with a pronounced tail in the positive region for the EP ENSO. In particular, the positive skewness of 1.3 indicates a tendency towards extreme positive events (rare but strong El Niño events, e.g., 1982–83, 1997–98, 2015–16). For the CP ENSO, the negative coefficients of skewness and kurtosis suggests a platykurtic distribution with a heavy tail in the negative region, indicating that it contains more data in the extremes compared to a normal distribution. In particular, the negative skewness value (–0.57) indicates a tendency for the CP ENSO to be more suited for representing cold events (La Niña), as negative SST anomalies (extreme negative events) are more frequent pronounced or persistent than positive ones.

The EP and CP ENSO cycles are an example of a "quasi-periodic" phenomenon. Wavelet methods — useful introductions are provided in [37] and [38] — have been widely used to analyse climatic data at multiple time scales because of their ability to identify the duration of dominant events or cycles within a signal [31,39–42]. The wavelet transform, using small, localized wave functions called wavelets, provides an adaptive time-frequency decomposition of the signal, where each frequency component displays a resolution matched to its scale. The localized nature of the wavelet basis function, and the flexibility of its windowing function, with the (localized) wavelet function dilated or compressed to simultaneously extract cycles at different frequencies, are especially useful for analyzing complex signals, that is signals that are "nonstationary, have short-lived transient components, have features at different scales, or have singularities" ([43], p.386).

The wavelet transform produces coefficients that represent the strength of the signal at different scales (frequencies) and locations. By squaring the absolute value of the wavelet coefficients, the sample wavelet power spectrum provides a representation of the energy density of the signal at each scale and location. Therefore, the wavelet transform determines which scales contribute most significantly to the signal's overall variance, revealing both the dominant modes of variability and how those modes vary over time.

Since estimated wavelet power spectra are biased in favour of large scales, the squared (absolute) values of CWT wavelet coefficients, denoted as $|W_x(s,u)|^2$, is divided by the corresponding scale based on the energy definition according to the bias rectification proposed by [44]. The (rectified) wavelet power spectra of the EP ENSO (left) and CP ENSO (right) are presented in Fig 2. The time-frequency plot in Fig 2 shows time recorded on the horizontal axis and periods, measured in quarters, on the vertical axis. The amount of signal energy contained at each specific scale and location is visualized by colour code, from dark blue (low power) to dark red (high power). Thus, regions with warmer colours correspond to areas with wavelet power coefficients of large magnitude. Visualizing the graph at a given scale (frequency), one can see how the power of the projection varies over time at that scale, while visualizing down the graph one can see how the power varies with the wavelet scale at a given point in time. The statistical significance of wavelet power coefficients is assessed using the cumulative areawise significance test developed by [45] to circumvent the multiple testing problem associated with the point-wise approach (further details are provided in S7 Appendix) firstly applied in [31]. A black contour line delimiting regions of 5% cumulative areawise significance against the null hypothesis of an autoregressive process of first order AR(1) is displayed. A red noise AR(1) process can be considered an acceptable noise background model for the global surface temperature [46,47], as many climatic variables have higher power at longer periods.

The left panel in Fig 2 shows that for the EP ENSO the largest wavelet power coefficients in the time-frequency plane are concentrated in the region between late 1970s and early 2000s at the 3–6 years frequency band. These results are consistent with the previous findings of intense events in the eastern Pacific occurred in 1982–83 and 1997–98. The right panel of Fig 2 shows that the CP ENSO has two dominant periods: one between the mid-1960s and late 1980s at the 1–4 years frequency band, and the other during the 2005–2015 period at the 2–4 years frequency range.

As expected, given that CP and EP measures are based on the EOF method, the statistically significant high-power regions for the EP and CP ENSO do not overlap. This wavelet finding is consistent with the observation that EP and CP ENSO events exhibit distinct SST patterns, one coincident with an anomalous warming area located in the eastern Pacific

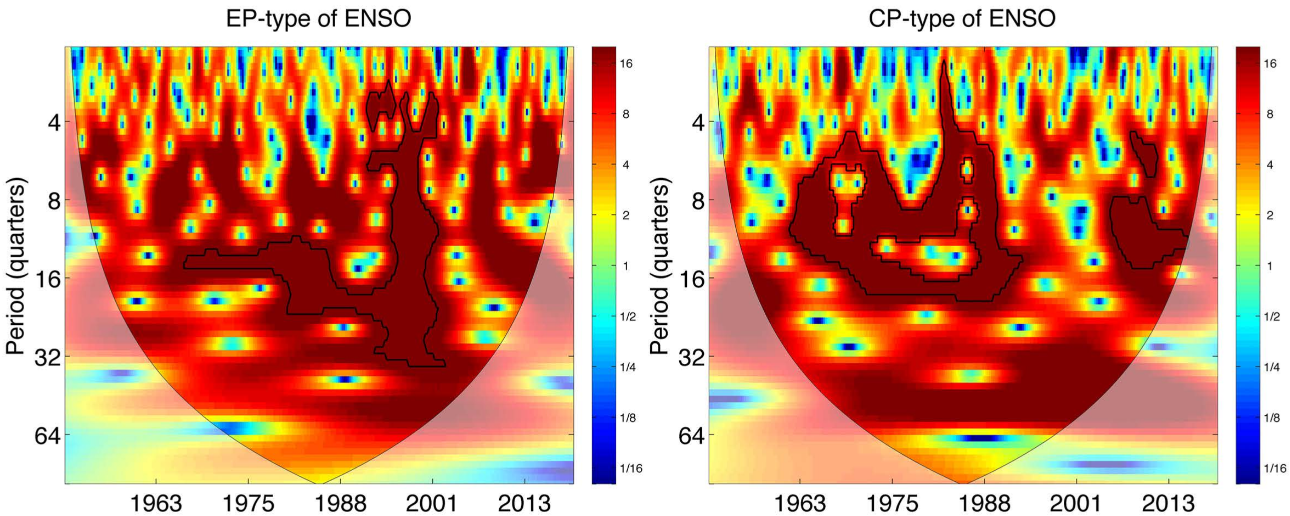

Fig 2. Wavelet power spectrum of EP (left) and CP (right) types of ENSO. *Note: Time is recorded on the horizontal axis and the scale of the wavelet transform on the vertical axis, with frequency converted to periods (quarters). The colour code for power ranges from dark blue (low power) to dark red (high power). A thick black contour encloses regions of 5% cumulative areawise significance. Light shading represents the cone of influence, i.e., the region in which edge effects cannot be ignored.*

https://doi.org/10.1371/journal.pclm.0000985.g002

and the other concentrated in the central Pacific [48,49]. Such differences in the time-frequency localization of high-power regions of the different types of ENSO events suggests that we can use the two series to identify independent effects from CP and EP ENSO shocks.

3. Effects of the EP and CP ENSO on inflation

3.1. Methodology and data

The multiscale pattern of the ENSO-inflation relationship, together with the non-stationary properties of the individual time series call for methods with the ability to manage scale-dependent, nonstationary relationships between time series. Wavelet coherence measures co-movement of two time series in the time-frequency space and allows us to study correlations between variables on multiple time scales and over different periods. Therefore, it allows for the detection of correlations that appear and disappear over time and can distinguish correlations occurring at different frequencies and over various time durations, such as short-lived events versus long-term influences. Indeed, the ENSO-inflation link may be strong in some episodes and weak in others, as recently noted in several empirical works on the asymmetrical effect of these climate cycles on macroeconomic variables [26,50,51].

To define wavelet coherence, we need to introduce the cross wavelet transform and cross wavelet power. Let W_x and W_y be the continuous wavelet transform of the signals x(.) and y(.). Their cross-wavelet power, given by $|W_{xy}| = |W_x W_y|$, depicts the local covariance of two time series at each scale and frequency [52]. The wavelet coherence is defined as the modulus of the wavelet cross spectrum normalized to the single wavelet spectra [46]:

$$R^2_{xy} = \frac{\left|S\left(s^{-1}W_{xy}(s,u)\right)\right|^2}{\left|S\left(s^{-1}W_x(s,u)\right)\right|\left|S\left(s^{-1}W_y(s,u)\right)\right|}$$

where $W_{xy}(s,u)=W_x W^*_y$ is the cross-wavelet transform and * indicates the complex conjugate, and S is a smoothing operator in both time and scale. The squared wavelet coherence coefficient R^2_{xy} is analogous to the squared correlation coefficient in linear regression. This normalized quantity, ranging from 0 and 1, measures the local correlation of two time series in the time-frequency space and can be used to detect the region where the two phenomena have strong local interactions. As for the wavelet power spectrum, regions of low and high coherency corresponding to areas of weak and strong local correlation are indicated by colour coding, with the colour code ranging from dark blue (low coherence) to dark red (high coherence).

Moreover, from the imaginary and real parts of the cross wavelet transform we have information about the relative position of the two series through the phase difference, defined as:

$$\phi_{xy} = tan^{-1}\left(\frac{\Im\left[W_{xy}(s,u)\right]}{\Re\left[W_{xy}(s,u)\right]}\right)$$

The wavelet phase difference between the two series charts lead/lag relationships by frequency, with the phase information graphically coded by arrows superimposed in regions characterised by high coherency. The direction of arrows shows the relative phasing between two time series and can be interpreted as indicating a lead/lag relationship: right arrows mean that the two variables are in-phase, while left arrows mean that the two variables are in-antiphase.

In order to derive our inflation measures, quarterly national price level data are transformed into their year-on-year quarterly growth rates — further details on our data sources are provided in S6 Appendix. Our dataset covers 23 advanced economies (Australia, Austria, Canada, Denmark, Finland, France, Germany, Greece, Ireland, Italy, Japan, Netherlands, New Zealand, Norway, Portugal, South Korea, Spain, Sweden, Switzerland, Taiwan, United Kingdom, United States) and 17 emerging countries (Argentina, Bolivia, Brazil, Chile, Colombia, Costa Rica, El Salvador, Guatemala, Honduras, India, Malaysia, Mexico, Pakistan, Peru, Philippines, Thailand, Uruguay) for the postwar period (1950:Q1–2019:Q4). This broad set of countries also allows us to consider countries that are directly affected by ENSO (e.g., Australia and Peru), countries that are strongly teleconnected by ENSO (e.g., Mexico, Thailand, and Malaysia) and countries that are weakly teleconnected (e.g., much of Europe). This study is based on a sample of countries for which consistent quarterly inflation data are available, which inevitably biases coverage toward higher-income, data-rich economies. This limitation reflects the inherent challenges of constructing long-span quarterly datasets, particularly for lower-income and tropical countries that are often more directly exposed to climate shocks. In S5 Appendix, we discuss the selection biases that arise from these data issues and the implications for ENSO-economy research.

The wavelet coherence plots in Figs 3 and 4 present the time-frequency relationship between the inflation rate and the two types of ENSO, EP and CP respectively, for a subset of countries (Figs A–E in S1 Appendix display the coherence results for all countries). Here, by way of example, we present a selection of countries from different geographical regions that exhibit statistically significant regions of coherence. Each panel in Figs 3 and 4 displays time on the horizontal axis, the scale on the vertical left axis, with periods measured in quarters, and a coloured vertical bar providing the correlation strength, between 0 and 1, displayed on the right axis. As before, the colour intensity represents the strength of coherence: red areas indicate high coherence, while blue areas show low coherence. The statistical significance of all wavelet coherence spectra is evaluated using the cumulative areawise test [45] to account for the simultaneous testing of multiple hypotheses. Thick black contours enclose regions of 5% cumulative areawise significance against the null hypothesis of an autoregressive process of first order AR(1). The shaded areas at the plot's edges represent the cone of influence, that is areas in the time-frequency plane where edge effects become significant, and results should be interpreted with caution. Arrows superimposed upon statistically significant regions show the phase relationship between the two variables: arrows pointing right (left) indicate in-phase (anti-phase) relationship, and up/down arrows represent a phase lag or lead. Specifically, right arrows pointing up (down) indicate that the ENSO cycle is positively related and lagging (leading) inflation. Left arrows pointing up (down) indicate that the ENSO cycle is negatively related and leading (lagging) inflation.

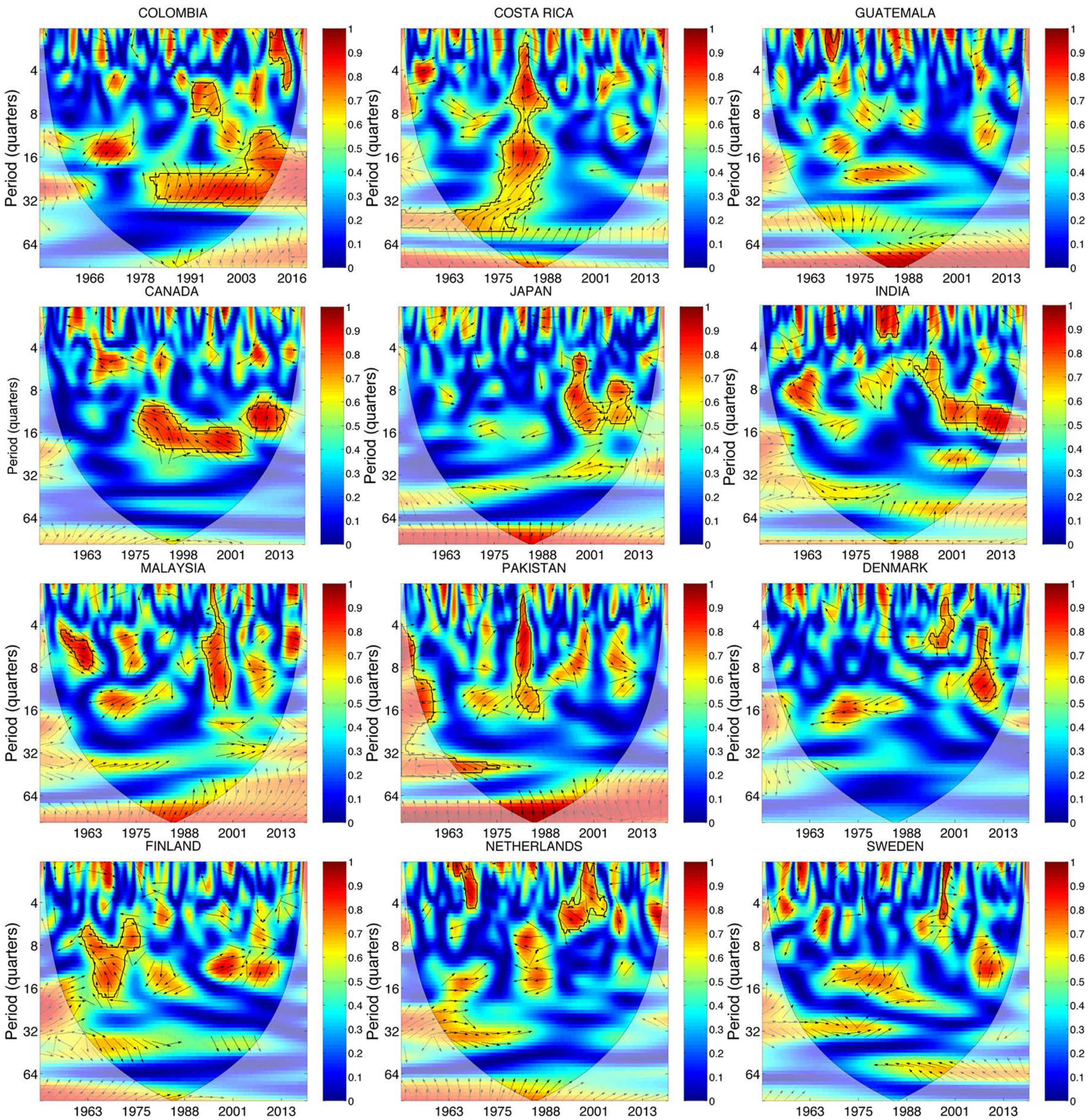

Fig 3. Wavelet coherence between EP ENSO and inflation. Note: Time is recorded on the horizontal axis and the scale of the wavelet transform on the vertical axis, with frequency converted to periods (quarters). The colour code for power ranges from dark blue (low coherence) to dark red (high coherence). A thick black contour encloses regions of 5% cumulative areawise significance. Right (left) arrow means that the two variables are in-phase (anti-phase): if the right arrow points up (down) EP ENSO is leading (lagging) inflation and if the left arrow points up (down), EP ENSO is lagging (leading) inflation. The results for all the countries of the sample are presented in Figs A–E in S1 Appendix.

https://doi.org/10.1371/journal.pclm.0000985.g003

3.2. EP ENSO effects on inflation

The wavelet coherence plots in Fig 3 exhibit a rich time-frequency structure indicating a complex, non-stationary, time-varying relationship between the ENSO cycle and national inflation rates. The presence of multiple regions of high coherence, coupled with their irregular distribution across both time and scales, suggests that the EP ENSO-inflation relationship displays significant time-heterogeneity. Moreover, the proportion of statistically significant regions — identified

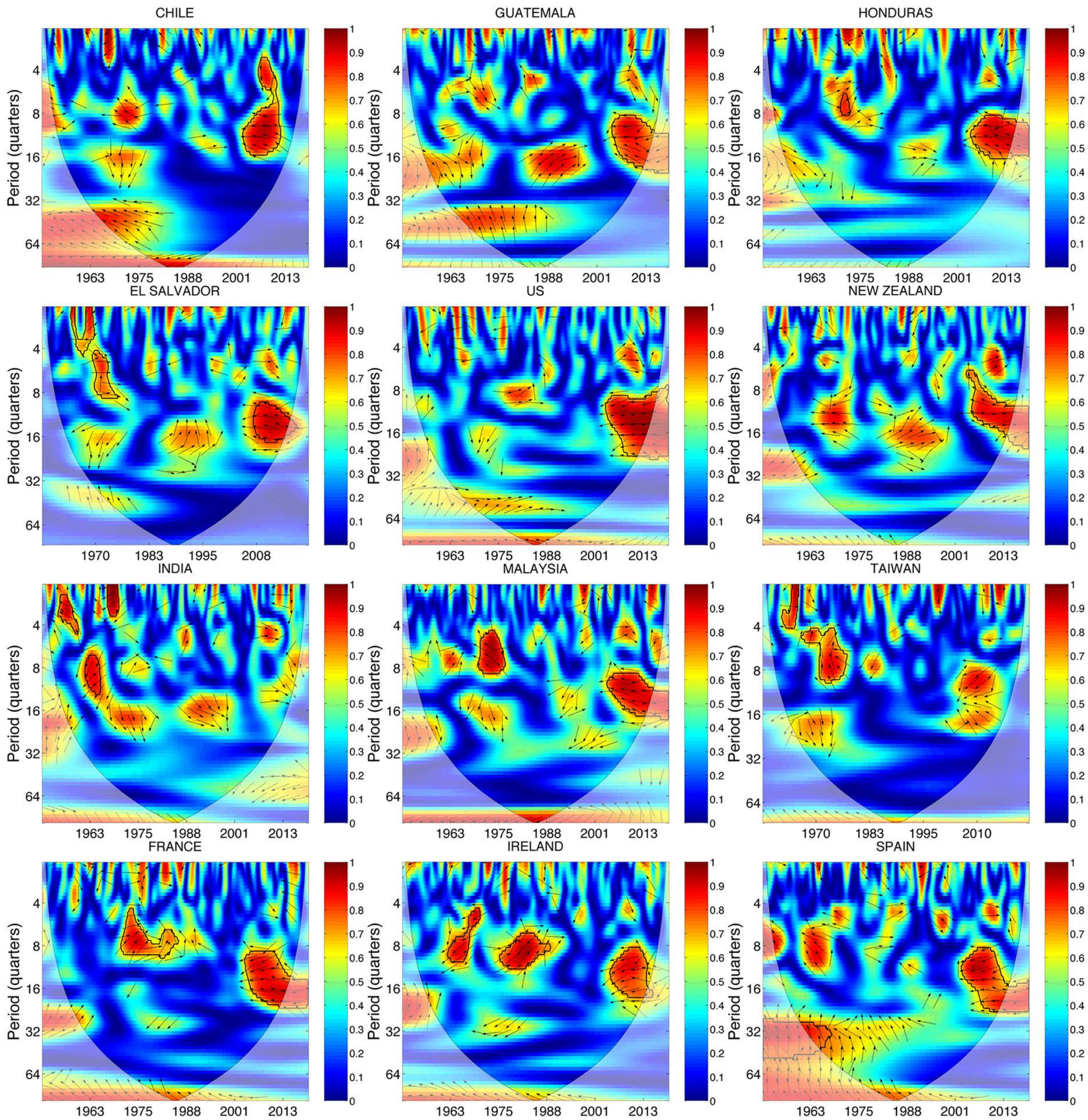

Fig 4. Wavelet coherence between CP ENSO and inflation. Note: Time is recorded on the horizontal axis and the scale of the wavelet transform on the vertical axis, with frequency converted to periods (quarters). The colour code for power ranges from dark blue (low coherence) to dark red (high coherence). A thick black contour encloses regions of 5% cumulative areawise significance. Right (left) arrow means that the two variables are in-phase (anti-phase): if the right arrow points up (down) CP ENSO is leading (lagging) inflation and if the left arrow points up (down), CP ENSO is lagging (leading) inflation. The results for all the countries of the sample are presented in Figs A–E in S1 Appendix.

https://doi.org/10.1371/journal.pclm.0000985.g004

through the cumulative areawise test — relative to high coherence areas is rather limited. Examining the country-specific features of the EP ENSO-inflation relationship we observe a generally weak or even absent link for several Latin American countries that are directly impacted by the EP ENSO cycle, such as Bolivia, Brazil, Chile, Peru (see Fig A in S1 Appendix). The main exception is Colombia, which exhibits several statistically significant regions across different frequency ranges. Statistically significant regions are also detected for Costa Rica — at scales of 1–6 years between the mid-1970s and mid-1980s — and for Mexico, between the mid-1980s and early-1990s. A number of time-localized regions of high coherence are detected at higher frequencies (less than 1 year) for several countries, including Honduras, El Salvador, Uruguay, Mexico and Guatemala — the latter being the only one with statistically significant coherence. The correlation patterns observed for North American countries differ substantially. Canada exhibits two statistically significant regions at the 2–4 years frequency band: one spanning from the mid-1980s to the early 2000s, and another during the mid-to-late 2000s. In contrast, the United States shows a single statistically significant region in the late 1950s at frequencies below 1.5 years.

The number of western Pacific and Asian countries displaying statistically significant high coherence regions is greater than that observed for Latin American countries. Statistically significant areas in the 1–4 year frequency range are detected for India, Japan, Korea, and Malaysia during the 1990s. Additional significant regions are found for India (at frequencies below 1 year during the 1980s and at 2–4 years from the early-2000s onward), Japan (at 2–4 years during the 2000s) and for Malaysia (at 1–2 years between the late 1950s and early 1960s). Pakistan also exhibits a statistically significant area in the early to mid-1980s at frequencies below 4 years. Although several high-coherence regions are identified for Australia, the Philippines, and Thailand, none of these are statistically significant. Finally, New Zealand and Taiwan display a generally weak relationship throughout the entire period.

The wavelet coherence plots for European economies align with the heterogeneous patterns observed in countries directly and indirectly affected by EP ENSO shocks. Statistically significant regions are detected for the Nordic countries and the Netherlands across different time scales and periods. Significant coherence is found in the early 1960s for the Netherlands at higher frequencies, and for Finland within the 1.5–4 years frequency range. Additional statistically significant areas at higher frequencies are identified for Denmark, the Netherlands, and Sweden around the mid-1990s. Both Denmark and the Netherlands exhibit further significant regions: the former at 1–4 years during the mid-to-late 2000s, and the latter at 1–2 years between the late 1980s and late 1990s.

Overall, the analysis highlights a markedly heterogeneous relationship between EP ENSO events and national inflation dynamics across countries. While some countries — such as Colombia, India, Japan, and several European economies — display statistically significant and temporally localized regions of high coherence, the majority show weak linkages. The frequency bands and time periods of significance vary widely, underscoring the absence of a common or persistent inflationary response to EP ENSO shocks. This heterogeneity suggests that the influence of EP ENSO on inflation operates through country-specific channels rather than a uniform global mechanism.

3.3. CP ENSO effects on inflation

The time-frequency analysis of the relationship between CP ENSO and inflation confirms that the effects are country-specific, yet it also reveals a notable common pattern. In particular, a statistically significant relationship emerges in the 2–4 years frequency band after c. 2000 — a feature that appears consistently across countries and aligns with the high-power, statistically significant region observed in the wavelet power spectrum of the CP-type of ENSO.

Among Latin American countries, the wavelet coherence results indicate three distinct periods of significant comovement between ENSO and inflation. The first occurs at higher frequencies (cycles below two years) from the mid-1960s to the early 1970s. Although many countries display elevated coherence during this period, it reaches statistical significance only for Honduras and El Salvador. The second period spans roughly the early 1980s to the late 1990s, with notable coherence at frequencies around four years in Argentina, Brazil, Guatemala, Mexico, and Peru; El Salvador shows only weak coherence in this band. A third and more recent phase appears from the early 2000s, particularly in Chile, Guatemala, Honduras, El Salvador, and, to a lesser extent, Costa Rica. Additionally, there is evidence of short-lived but noticeable time-localized effects at higher frequencies (less than one year) for several countries — including Chile, Colombia, Costa Rica, Guatemala, Honduras, Mexico, El Salvador, and Uruguay — concentrated mainly before the 1980s.

The strong coherence pattern observed within the 2–4 years frequency range also appears in North American and Oceanian countries, although it does not reach statistical significance for Australia. Statistically significant CP ENSO effects in the 2–4 years band during the first decade of the 2000s are detected across several Asian countries, including Japan, Pakistan, Malaysia, and Thailand. This high-coherence region is also present in the Philippines, Taiwan, and, to a lesser extent, Korea, but not in India, where significant coherence occurs instead at higher frequencies — below 1 year and around 2 years. Additionally, Malaysia and Taiwan display a high-coherence region in the 1–2 years frequency band in the early 1970s.

The patterns emerging from the bottom panels of Fig 4 are particularly striking. Nearly all European countries — except the Netherlands and Norway, and to a lesser extent Portugal and Switzerland — exhibit a large, statistically significant high-coherence region in the first decade of the 2000s within the 2–4 years frequency range. Smaller statistically significant areas also appear at high frequencies (less than 2 years) for a limited number of countries: Ireland in the mid-1960s, France and Ireland from the early 1970s to the mid-1980s, and Portugal in the late 1960s.

In S2 Appendix, we also present the wavelet coherence relationship between ENSO and global commodity prices, focusing on energy and non-energy commodity prices. Fig A in S2 Appendix presents the wavelet coherence plots between CP (left panels) and EP (right panels) measures of the ENSO cycle and energy and non-energy commodity price indices. The results show major differences between energy and non-energy commodity prices — whilst for global energy prices there are few significant areas concentrated both in time and frequencies, for non-energy commodity prices high coherence regions are widespread both over time and across frequencies.

3.4. Summary of findings

The main uniformity is the negative effect of CP on inflation at the 2–4 year statistically significant area displayed after mid-2000s by most countries of our sample. Positive effects are less numerous and more associated to EP events, e.g., Costa Rica, India (at shorter time scales), Japan, Korea, Malaysia, Denmark, Germany and Netherlands, mostly at scales lower than 2 years. These findings are consistent with the literature that relates the observed nonlinearities in the ENSO pattern, in the context of the different amplitude of ENSO warm and cold phases [35,53], to "ENSO diversity", with the EP ENSO characterised by stronger warm-than-cold SST anomalies, and the CP ENSO by larger cold-than-warm SST anomalies.

Overall, the results presented in this section suggest a multiscale, time-localized, transient and country-specific relationship. The multiscale nature of the relationship between ENSO and inflation is clearly evident in the wavelet coherence plots, as statistically significant (but also high-coherence) areas are detected at shorter-term frequencies, up to 1-year, but also at frequencies between 1 and 2 years and at the 2–4 years frequency range. These periods of strong correlation are widely dispersed in the time-frequency map, restricted to some specific periods and short-lived, therefore suggesting the transient effects of ENSO events on inflation.

4. A global vector autoregression model of the ENSO-inflation relationship

Wavelet coherence analysis shows that the relationship between the ENSO cycle and national inflation rates displays episodic features — statistical significance is specific to particular time-periods and frequencies. There is also extensive evidence that the ENSO cycle affects global commodity prices [1,3,21,54], which will have global effects on national inflation. To evaluate the ENSO-inflation relationship in a multivariate framework we employ the GVAR methodology — the technical aspects of the GVAR methodology are detailed in [3] and [55]. [56] have noted the "over-controlling problem", resulting from climate variables impacting on other control variables in economic models. This problem implies there may be a bias in the estimates if we control for other economic variables that are affected by climate (such as global commodity prices) when attempting to identify the effects of climate, resulting in bad controls [57]. At the same time we do not know whether there is an omitted variable bias by excluding these variables. The GVAR model deals with this problem by modelling a system of variables affected by climate shocks that are interacting with each other. The GVAR model implies that although the "over-controlling problem" may exist, the complex interactions between climate and economy means that some conditioning has to be considered in the modelling process.

The GVAR methodology allows us to model the effect of a global variable (in this case the ENSO process) on national economies that are inter-related in the global economy via trade and capital flows [55,58–60]. The GVAR framework has three important useful features: first, global shocks, such as the ENSO variations that affect many parts of the world either directly or via teleconnections can be modelled as global shocks to an economic system; second, global inter-relatedness of economies is at the heart of GVAR models, allowing us to model the effects of a global shock on the world economy (defined here as a set of inter-related economies); third, unlike standard panel models, GVAR models estimate heterogeneous effects across countries. A set of trade weights captures the cross-national linkages, allowing us to model spillover effects across countries; moreover, these weights change over time, allowing us to capture temporal changes in global linkages.

[3] have applied the GVAR framework to estimate the macroeconomic effects of El Niño fluctuations on 21 economies/regions of the global economy using quarterly data for the period 1979:Q2–2013:Q1. We contribute to the GVAR evaluation of the ENSO cycle in a number of ways. First, we complement the work of [3] by focusing on the implications of ENSO diversity; since EP and CP ENSO variations affect teleconnections in different ways, we expect this feature to result in different economic effects on individual countries and global variables, such as world commodity prices. Second, we extend the quarterly data set to consider a longer time period, from 1960 to 2019, allowing us to capture more ENSO cycles; although the coherence analysis can use national inflation rates from c.1950 at quarterly frequency, several control variables required for the GVAR are only available from c.1960, which fixes the start of the GVAR sample. Given the length of time period, we also allow for changes in trade weights to capture how economic spillovers evolve over long historical periods since the 1950s.

An innovation in our study is to combine the wavelet methodology and the GVAR framework. This allows us to focus on the impacts of specific frequencies of the ENSO cycle within a GVAR model. To complement the wavelet analysis of the first part of this study we use the wavelet methodology to decompose the ENSO cycle applying the maximal overlap discrete wavelet transform (MODWT), which uses discretized versions of the dilation and location parameters of the wavelet basis filter. The MODWT decomposes the original signal into a limited number of different time scale components, each corresponding to a specified frequency band. With quarterly data a 4-level decomposition produces four wavelet details vectors d_1, d_2, d_3, and d_4, each associated with oscillatory variations on various timescales, 2–4, 4–8, 8–16, and 16–32 quarters, respectively, and one wavelet smooth vector, S_4 capturing fluctuations longer than 32 quarters. Since the dominant ENSO cycle is between 2–7 years, we take the sum of d_3 and d_4 variations to represent the cyclical properties of the ENSO cycle and use this information to evaluate the effects from ENSO shocks.

To implement the GVAR model we use a quarterly data set for 26 countries for the period 1960:Q1–2019:Q4, since the data for a number of control variables start in1960. The data set includes quarterly data on GDP, CPI inflation, effective exchange rates, global oil prices, global non-oil commodity prices, and measures of CP and EP ENSO variations (the data sources are described in S6 Appendix). The country coverage includes Argentina, Australia, Austria, Belgium, Brazil, Canada, Chile, Finland, France, Germany, India, Italy, Japan, Korea, Mexico, Netherlands, Norway, New Zealand, Philippines, South Africa, Spain, Sweden, Switzerland, Turkey, United Kingdom and the United States. The 26 countries are a subset of the 40 countries we considered using wavelets analysis. The more limited selection of countries reflects the availability of reliable and consistent quarterly macroeconomic data, which inevitably biases coverage toward higher-income, data-rich economies. As a result, several countries significantly affected by the ENSO cycle — such as Peru, Ecuador, and Indonesia — cannot be included in a GVAR analysis. Nevertheless, the 26-country sample employed here encompasses a broad set of economies influenced by ENSO either directly or through climate teleconnections. Furthermore, the GVAR framework captures global economic interdependencies by incorporating trade-weighted linkages across countries. An important advantage of this sample is that it represents a substantial share of global income, thereby enabling the estimation of worldwide economic effects associated with ENSO. These data reliability issues are discussed further in S5 Appendix.

In Fig 5 we consider the effects of CP ENSO cycle shock as captured by the sum of the d_3 and d_4 movements — we also considered the effect of high frequency shock to the CP ENSO cycle by considering the movements of d_1 and d_2 decompositions. The only significant national inflation effects are for India (+0.24 per cent by Q4) and Mexico (+0.6 per cent by Q2); world non-oil commodity prices are unaffected and world real oil prices fall (−3.0 per cent by Q12). To account for differences in intensity and temporal dynamics of the CP and EP ENSO, we define El Niño shocks in our model as one-standard-deviation innovations (over the whole sample period 1960–2019) to the respective $d_3 + d_4$ cycles of the (orthogonalised) CP and EP indices, rather than imposing a uniform shock size or duration across event types. This is the common practice in econometric estimations. Estimating the effect of one standard deviation shock to a CP ENSO cycle we observe a significant positive effect on CPI inflation in India (0.5 per cent by Q4) and Mexico (1.0 per cent by Q4); we observe a negative effect on New Zealand (–0.2 per cent by Q4). The point estimates for Argentina and Australia are also negative but are not statistically significant at the 90% level over the horizons considered. The effect on oil prices is negative (-2.0 per cent) and statistically significant over a 4-Quarter time-profile (Fig 6); the effect on non-oil commodity

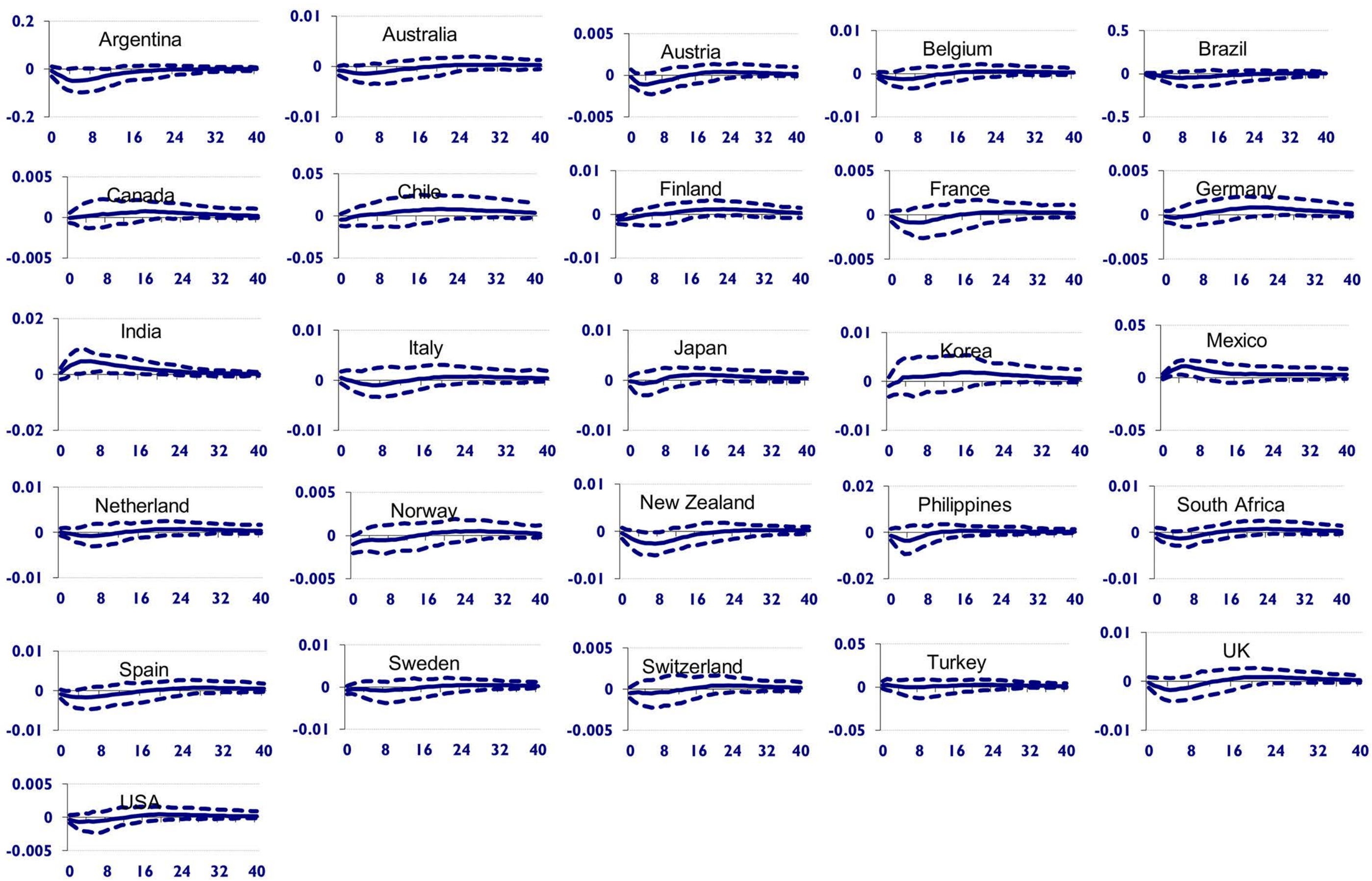

Fig 5. Impulse Responses of Inflation to CP ENSO Cycle Shock. Note: The Y-axis shows the deviation from baseline (where 0.01 equals 1 percentage point). The X-axis represents the quarters after the shock (horizon). The solid line is the median estimate of the impulse response, and the dashed lines indicate the 90% confidence bands obtained via bootstrap.

https://doi.org/10.1371/journal.pclm.0000985.g005

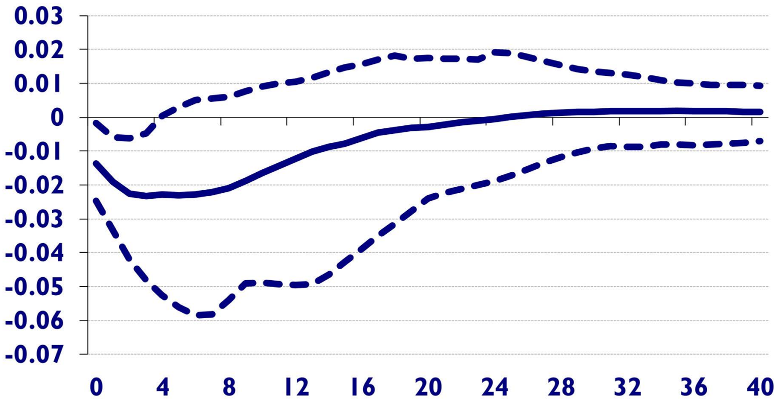

Fig 6. Impulse Responses of World Real Oil Price to CP ENSO Cycle Shock. Note: The Y-axis shows the deviation from baseline (where 0.01 equals 1 percentage point). The X-axis represents the quarters after the shock (horizon). The solid line is the median estimate of the impulse response, and the dashed lines indicate the 90% confidence bands obtained via bootstrap.

https://doi.org/10.1371/journal.pclm.0000985.g006

prices is positive (1.0 per cent by Q12) but not statistically significant over a 3-year horizon (Fig 7). As a robustness check, we re-estimated using the full (non-decomposed) CP series; the results are very similar, suggesting the cyclical decomposition captures most of the CP variation. In reporting GVAR impulse responses, we present 90% bootstrapped confidence intervals. This choice reflects standard practice in the GVAR literature and aligns with closely related work, including [3], who also report 5%–95% bootstrapped error bounds and, additionally, 16%–84% bounds corresponding to one-standard-deviation confidence intervals. The choice of working with the 90% confidence level in GVAR analysis reflects the objective of characterising the dynamic response patterns and cross-country transmission mechanisms in a large, interconnected system, where more conservative thresholds can substantially reduce power. Accordingly, our interpretation of results does not hinge on marginal statistical significance at individual horizons, but on the sign, persistence, and coherence of responses across countries and variables.

Given the multi-country nature of the GVAR, a large number of impulse responses are produced. We therefore avoid interpreting the output as a collection of independent hypothesis tests. Standard multiple-comparison corrections (e.g.,

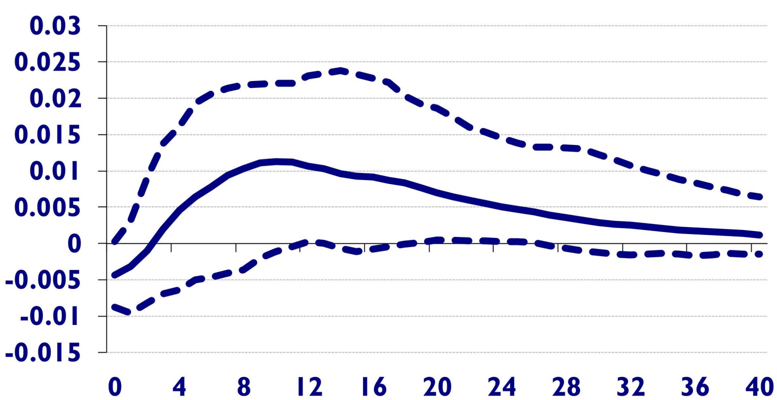

Fig 7. Impulse Responses of World Non-Oil Commodity Real Price to CP ENSO Cycle Shock. Note: The Y-axis shows the deviation from baseline (where 0.01 equals 1 percentage point). The X-axis represents the quarters after the shock (horizon). The solid line is the median estimate of the impulse response, and the dashed lines indicate the 90% confidence bands obtained via bootstrap.

https://doi.org/10.1371/journal.pclm.0000985.g007

Bonferroni-type adjustments) are designed for sets of independent tests and would be overly conservative and difficult to interpret in a system where responses are jointly determined through global linkages. Instead, we emphasise systematic patterns — such as differences between CP and EP shocks that are consistent across horizons and country groups — and cross-method consistency with the wavelet evidence. Where responses are sensitive to the confidence level, we state this explicitly and avoid over-interpreting borderline cases.

The effects of the EP ENSO cycle are more muted (see Fig 8). Estimating the effect of one standard deviation shock to the EP ENSO cycle we observe a significant positive effect on CPI inflation only for India (0.3 per cent by Q9). The effects on global oil prices and non-oil commodity prices are statistically insignificant (Figs 9 and 10). We also considered the effect of high frequency shock to the EP ENSO cycle by considering the movements of d_1 and d_2 decompositions — all national inflation effects are statistically insignificant, as are the effects on global commodity prices.

To evaluate the robustness of our findings and to assess the value added by modelling ENSO diversity, we conduct a set of sensitivity tests. First, we re-estimate the GVAR using the Niño 3.4 index, which pools ENSO activity into a single fixed-region measure and therefore removes the distinction between CP and EP events. The only change in this specification is the ENSO shock variable. All other elements of the model, including country-specific equations, foreign variables, lag structure, estimation method, and bootstrap inference, remain identical. This pooled specification can be viewed as a

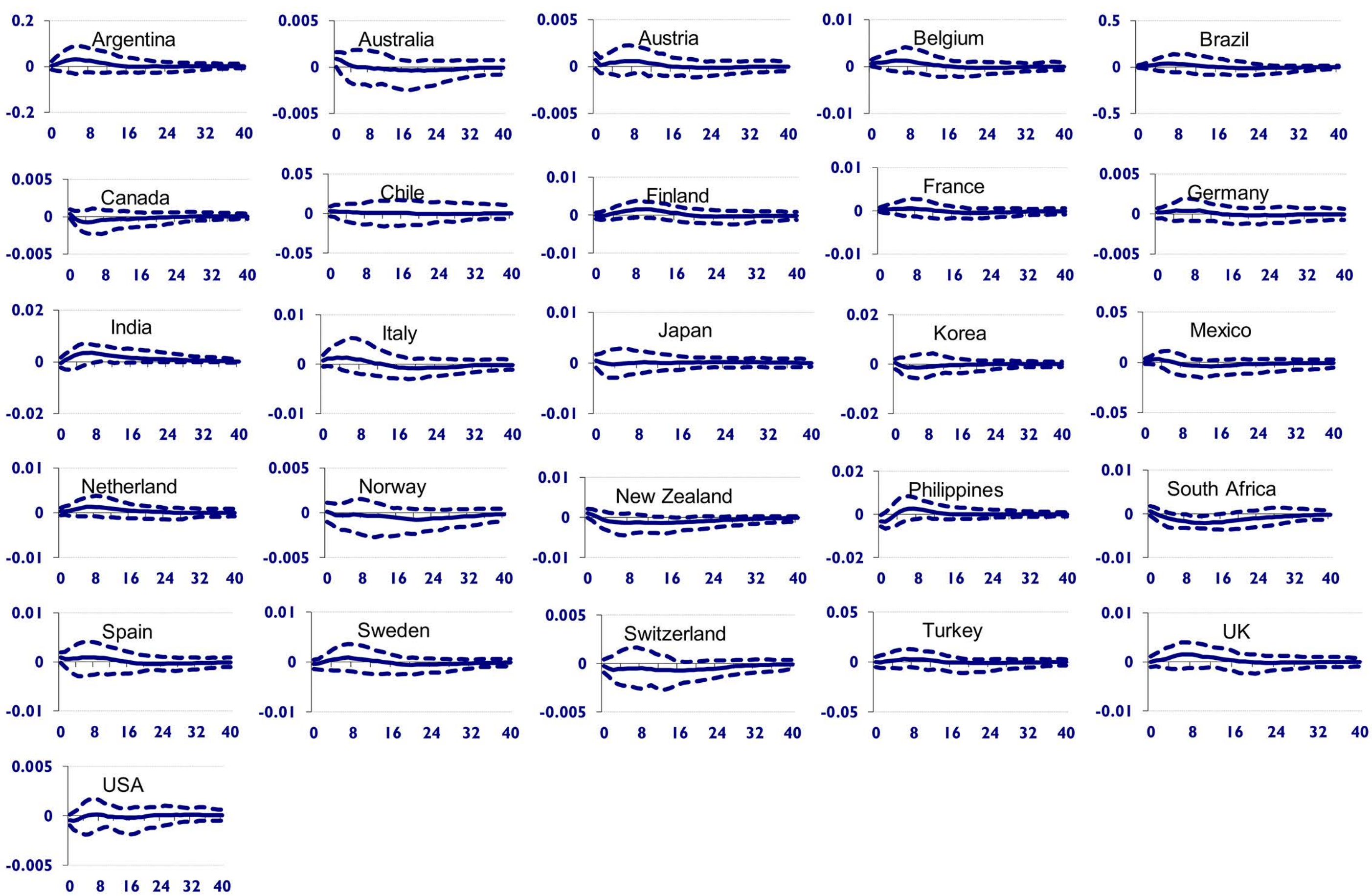

Fig 8. Impulse Responses of Inflation to EP ENSO Cycle Shock. Note: The Y-axis shows the deviation from baseline (where 0.01 equals 1 percentage point). The X-axis represents the quarters after the shock (horizon). The solid line is the median estimate of the impulse response, and the dashed lines indicate the 90% confidence bands obtained via bootstrap.

https://doi.org/10.1371/journal.pclm.0000985.g008

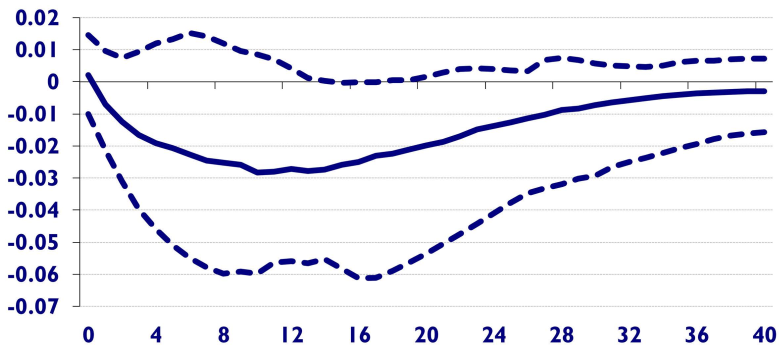

Fig 9. Impulse Responses of World Real Oil Price to EP ENSO Cycle Shock. Note: The Y-axis shows the deviation from baseline (where 0.01 equals 1 percentage point). The X-axis represents the quarters after the shock (horizon). The solid line is the median estimate of the impulse response, and the dashed lines indicate the 90% confidence bands obtained via bootstrap.

https://doi.org/10.1371/journal.pclm.0000985.g009

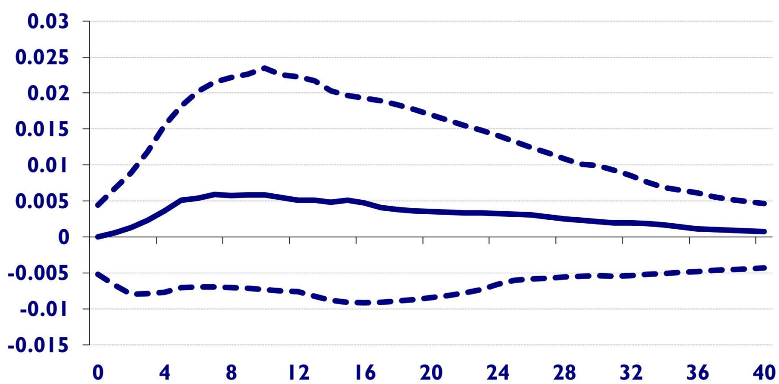

Fig 10. Impulse Responses of World Non-Oil Commodity Real Price to EP ENSO Cycle Shock. Note: The Y-axis shows the deviation from baseline (where 0.01 equals 1 percentage point). The X-axis represents the quarters after the shock (horizon). The solid line is the median estimate of the impulse response, and the dashed lines indicate the 90% confidence bands obtained via bootstrap.

https://doi.org/10.1371/journal.pclm.0000985.g010

more restrictive nested benchmark relative to our preferred CP and EP framework because it imposes the restriction that all ENSO events transmit through the same aggregate index and therefore cannot generate type-specific macroeconomic responses.

The Niño 3.4 results are summarised in S3 Appendix, which reports the responses of four-quarter CPI inflation, world real oil prices, and world real non-oil commodity prices to a one-standard-deviation Niño 3.4 shock. The estimated effects on global oil and non-oil commodity prices are broadly comparable in magnitude to those obtained from the CP and EP specifications, with similar sign, persistence, and overall shape of the response across horizons. At the country level, however, the comparison is more nuanced. The cross-country pattern of CPI responses differs across the two specifications: for some countries (e.g., Argentina, Korea, Mexico, New Zealand, and South Africa) the magnitude of the inflation response is larger when CP and EP shocks are modelled separately, while for others (e.g., Turkey, the USA, Canada, Finland, and Germany) the magnitude is larger under the pooled Niño 3.4 shock. Statistically significant Niño 3.4 responses at the 90% level are identified for India (0.6 per cent by Q4) and Germany (0.1 per cent by Q5). What the pooled Niño 3.4 specification cannot recover is the type-specific heterogeneity that emerges when CP and EP shocks are separated: the contrast between the more pronounced CP responses and the more muted EP responses reported in the main text is, by construction, absorbed into a single average effect under Niño 3.4. In light of the wavelet evidence and the CP/EP results presented in the main text, this comparison reinforces our reading that distinguishing ENSO types is informative for understanding the macroeconomic effects of El Niño and La Niña, while individual country-level magnitudes remain sensitive to the choice of ENSO measure.

Second, we consider whether nonlinearity matters to the estimates that we report using the GVAR model. To evaluate possible nonlinear effects, we have separated out the two different phases of the ENSO cycle into El Niño and La Niña states. For these different phases of the cycle, we estimate the GVAR models separately for the positive and negative phases of the ENSO cycle to identify nonlinear effects the El Niño and La Niña states (estimation results are reported in S4 Appendix). Our key finding here is that the linear model provides a good approximation — although some nonlinear effects are identified. Clearly the aspect of nonlinear effects needs further analysis using techniques that can comment more explicitly on modelling nonlinear features.

5. Discussion and conclusions

A number of key conclusions arise from this study. First, the wavelet coherence analysis has identified periods of strong coherence between CPI inflation and the ENSO cycle. We have focused on the importance of ENSO diversity and have shown that the CP and EP ENSO variations have differentiated effects across countries and frequencies. A key result from the wavelet coherence analysis is that the effects are significant but clearly episodic, with statistical significance confined to particular time periods and frequencies that also vary by country. Moreover, the significant episodes overlap over different phases of the ENSO cycle — El Niño and La Niña phases are both important determinants of inflation. A similar episodic relationship has also been identified for global commodity prices.

Second, when using the GVAR econometric methodology to identify effects on national inflation and global commodity prices, the significant effects are more limited, reflecting the episodic nature of significance identified using wavelet coherence. Combining the wavelet methodology with the GVAR framework allows us to comment on the specific frequencies affecting inflation. Estimating the effect of one standard deviation shock to a CP ENSO cycle (measured as fluctuations in the wavelet frequencies d_3 and d_4) we observe a significant positive effect on CPI inflation in India and Mexico and significant negative effects on New Zealand. The time-profile of the effect on non-oil commodity prices is positive (+1.0 per cent by Q12) but remains statistically insignificant across a 3-year period; the effect on oil prices is negative (–2.0 per cent) and statistically significant over the first 4-quarters of a shock.

This rich set of results show that ENSO diversity matters — linking the inflation effects of the ENSO cycle to ENSO diversity shows the complexity of modelling the economic processes involved. Wavelet coherence is a flexible tool that allows us to describe how ENSO diversity affects economic outcomes. In using GVAR to summarise the ENSO effects, we need to emphasise that we are seeking to evaluate the significance of an average relationship across the whole period of analysis (in our case 1960–2019). The fact that only a few national relationships are identified as being statistically significant needs to be interpreted with care in light of temporal shifts in the significance of the relationship as illustrated by the wavelet coherence analysis. The concept of statistical significance captured by wavelet analysis is also meaningful when analysing ENSO effects — we observe episodes of statistical significance between ENSO and CPI inflation across many countries and global oil and global commodity prices.

Using the GVAR methodology to determine magnitudes, we find that a one-standard-deviation shock to a CP ENSO cycle has statistically insignificant effects on real non-oil commodity prices. [1] found that a one-standard-deviation El Niño surprise causes an increase of 3.5 to 4 per cent in commodity prices. The differences here could be explained by differences in the type of econometric model used, the disaggregation of commodity prices, and the specific ENSO measure. Our specification of the GVAR is a more general specification than the VAR model used by [1], capturing important global interactions, and the importance of ENSO diversity is clear in the set of results presented in this paper. The evidence clearly suggests that the response of oil prices and non-oil commodity prices differ. In addition, the results reported in S4

Appendix that consider nonlinear effects for the different states of the ENSO cycle suggest that nonlinearity is important when analysing global commodity price effects.

Our results point to a number of areas for future research. First, our results highlight two aspects of statistical significance that researchers need to keep in mind when thinking about the ENSO-economy interactions. The non-parametric wavelet methods have identified episodes of statistical significance for most of the 40 countries we consider using wavelet coherence analysis; the parametric GVAR methods identify average effects across the whole sample period on some countries and effects on global commodity prices. Both sets of results contain important information. These time-varying effects are likely to be even more important across longer time periods as economies undergo structural (the sectoral shares of economies have changed significantly over time), institutional (the monetary institutions responding to inflation shocks have changed over time), informational changes (our knowledge of the ENSO cycle has improved over time) that may affect the impact of ENSO variations on national inflation and global commodity prices. Second, as the scientific understanding of the ENSO process has developed and our monitoring of the process in real time has improved, we expect some feedback on financial markets and policy makers that may affect the transmission process of ENSO variations to inflation. Financial markets may act to amplify the effect of ENSO variations via the futures commodity markets. At the same time central banks may learn to react to ENSO shocks as short-term supply-side shocks. ENSO diversity opens up a whole set of new research questions.

Supporting information

S1 Appendix. Wavelet coherence between inflation and ENSO across countries.
(DOCX)

S2 Appendix. ENSO effects on global commodity prices.
(DOCX)

S3 Appendix. Inflation effects estimated using the Niño 3.4 index.
(DOCX)

S4 Appendix. Nonlinear inflation effects of El Niño and La Niña events.
(DOCX)

S5 Appendix. Data reliability and measurement.
(DOCX)

S6 Appendix. Data sources for the quarterly dataset.
(DOCX)

S7 Appendix. Wavelet methodology and statistical significance.
(DOCX)

Author contributions

Conceptualization: Marco Gallegati, Solomos Solomou.

Data curation: Marco Gallegati.

Formal analysis: Marco Gallegati, Kun Tian.

Methodology: Marco Gallegati, Solomos Solomou, Kun Tian.

Software: Marco Gallegati, Kun Tian.

Supervision: Solomos Solomou.

Writing – original draft: Marco Gallegati, Solomos Solomou, Kun Tian.

Writing – review & editing: Marco Gallegati, Solomos Solomou.

References

1. Brunner AD. El Niño and world primary commodity prices: warm water or hot air? Rev Econ Stat. 2002;84:176–83.
2. Laosuthi T, Selover DD. Does El Niño affect business cycles? East Econ J. 2007;33:21–42.
3. Cashin P, Mohaddes K, Raissi M. Fair weather or foul? The macroeconomic effects of El Niño. J Int Econ. 2017;106:37–54. https://doi.org/10.1016/j.jinteco.2017.01.010
4. Dufrenot G, Ginn W, Pourroy M. Climate pattern effects on global economic conditions. Econ Model. 2024;141:106920.
5. Ginn W. ENSO-augmented Phillips curve: evidence from panel local projections. Oxf Bull Econ Stat. 2025. https://doi.org/10.1111/obes.70024
6. Yu JY, Kao HY. Decadal changes of ENSO persistence barrier in SST and ocean heat content indices: 1958-2001. J Geophys Res. 2007;113:D13106.
7. McPhaden MJ, Santoso A, Cai W. El Niño Southern Oscillation in a changing climate. Geophysical Monograph 253. In: McPhaden MJ, Santoso A, Cai W, editors. Washington, DC: American Geophysical Union; 2020.
8. Capotondi A, Wittenberg AT, Kug JS, Takahashi K, McPhaden MJ. ENSO diversity. In: McPhaden MJ, Santoso A, Cai W, editors. El Niño Southern Oscillation in a changing climate. Geophysical Monograph 253. Washington, DC: American Geophysical Union; 2020. p. 65–86.
9. Dieppois B, Capotondi A, Pohl B, Chun KP, Monerie P-A, Eden J. ENSO diversity shows robust decadal variations that must be captured for accurate future projections. Commun Earth Environ. 2021;2(1):212. https://doi.org/10.1038/s43247-021-00285-6
10. Geng T, Cai W, Wu L, Santoso A, Wang G, Jing Z, et al. Emergence of changing Central-Pacific and Eastern-Pacific El Niño-Southern Oscillation in a warming climate. Nat Commun. 2022;13(1):6616. https://doi.org/10.1038/s41467-022-33930-5 PMID: 36379936
11. Kao H-Y, Yu J-Y. Contrasting Eastern-Pacific and Central-Pacific Types of ENSO. J Clim. 2009;22(3):615–32. https://doi.org/10.1175/2008jcli2309.1
12. Yu JY, Lu MM, Kim ST. A change in the relationship between tropical central Pacific SST variability and the extratropical atmosphere around 1990. Environ Res Lett. 2012;7:034025.
13. Alizadeh O. A review of ENSO teleconnections at present and under future global warming. Wiley Interdiscip Rev Clim Change. 2024;15:e861.
14. Hansen JW, Hodges AW, Jones JW. ENSO Influences on Agriculture in the Southeastern United States*. J Clim. 1998;11(3):404–11. https://doi.org/10.1175/1520-0442(1998)011<0404:eioait>2.0.co;2
15. Adams R, Chen C, McCall B, Weiher R. The economic consequences of ENSO events for agriculture. Clim Res. 1999;13:165–72.
16. Iizumi T, Luo J-J, Challinor AJ, Sakurai G, Yokozawa M, Sakuma H, et al. Impacts of El Niño Southern Oscillation on the global yields of major crops. Nat Commun. 2014;5:3712. https://doi.org/10.1038/ncomms4712 PMID: 24827075
17. Ubilava D. El Niño, La Niña, and world coffee price dynamics. Agric Econ. 2012;43:17–26.
18. Ubilava D. The ENSO Effect and Asymmetries in Wheat Price Dynamics. World Dev. 2017;96:490–502. https://doi.org/10.1016/j.worlddev.2017.03.031
19. Dufrénot G, Ginn W, Pourroy M. Climate change impacts on commodity price stability through changing ENSO patterns. World Dev. 2026;197:107165. https://doi.org/10.1016/j.worlddev.2025.107165
20. Huang Y, Shu M, Liu F, Liu B, Huang C, Wang S. Nonlinear heterogeneity impact of El Niño Southern Oscillation on energy markets: a global perspective analysis. Energy. 2025;333:137475.
21. Ubilava D. The role of El Niño Southern Oscillation in commodity price movement and predictability. Am J Agric Econ. 2018;100:239–63.
22. Dufrenot G, Ginn W, Pourroy M. The effect of ENSO shocks on commodity prices: a multi-time scale approach. AMSE Working Paper No. 30. Marseille: Aix-Marseille School of Economics; 2021.
23. Hsiang SM, Meng KC, Cane MA. Civil conflicts are associated with the global climate. Nature. 2011;476(7361):438–41. https://doi.org/10.1038/nature10311 PMID: 21866157
24. Hsiang SM, Burke M, Miguel E. Quantifying the influence of climate on human conflict. Science. 2013;341(6151):1235367. https://doi.org/10.1126/science.1235367 PMID: 24031020
25. Hastings JV, Ubilava D. Agricultural roots of social conflict in Southeast Asia. J Peace Res. 2025;62:1714–32.
26. Smith SC, Ubilava D. The El Niño Southern Oscillation and economic growth in the developing world. Glob Environ Change. 2017;45:151–64. https://doi.org/10.1016/j.gloenvcha.2017.05.007
27. Romero JV, Naranjo-Saldarriaga S. Weather shocks and inflation expectations in semi-structural models. Lat Am J Cent Bank. 2024;5:100112.
28. Keppenne CL. An ENSO Signal in Soybean Futures Prices. J Clim. 1995;8(6):1685–9. https://doi.org/10.1175/1520-0442(1995)008<1685:aesisf>2.0.co;2
29. Ferreira GLM, Tonin JM, Alves AF. Impacts of El Niño southern oscillation on hedge strategies for Brazilian corn and soybean futures contracts. Rev Econ Sociol Rural. 2022;60(spe). https://doi.org/10.1590/1806-9479.2021.250643

30. Trenberth KE. Spatial and temporal variations of the Southern Oscillation. Q J R Meteorol Soc. 1976;102(433):639–53. https://doi.org/10.1002/qj.49710243310
31. Torrence C, Compo GP. A Practical Guide to Wavelet Analysis. Bull Amer Meteor Soc. 1998;79(1):61–78. https://doi.org/10.1175/1520-0477(1998)079<0061:apgtwa>2.0.co;2
32. Capotondi A, Wittenberg AT, Newman M, Di Lorenzo E, Yu JY, Braconnot P, et al. Understanding ENSO diversity. Bull Am Meteorol Soc. 2015;96:921–38.
33. Choi KY, Vecchi GA, Wittenberg AT. ENSO transition, duration, and amplitude asymmetries: role of the nonlinear wind stress coupling in a conceptual model. J Clim. 2013;26:9462–76.
34. Kug JS, Jin FF, An SI. Two types of El Niño events: cold tongue El Niño and warm pool El Niño. J Clim. 2009;22:1499–515.
35. Dommenget D, Bayr T, Frauen C. Analysis of the nonlinearity in the pattern and time evolution of El Niño Southern Oscillation. Clim Dyn. 2013;40:2825–47.
36. Yu JY, Kim ST. Three evolution patterns of central-Pacific El Niño. Geophys Res Lett. 2010;37:L08706.
37. Percival DB, Walden AT. Wavelet methods for time series analysis. Cambridge: Cambridge University Press; 2000.
38. Gençay R, Selçuk F, Whitcher B. An introduction to wavelets and other filtering methods in finance and economics. San Diego: Academic Press; 2002.
39. Lau KM, Weng H. Climate signal detection using wavelet transform: how to make a time series sing. Bull Am Meteorol Soc. 1995;76:2391–402.
40. Sonechkin DM, Datsenko NM. Wavelet analysis of nonstationary and chaotic time series with an application to the climate change problem. Pure Appl Geophys. 2000;157:653–77.
41. Lin Y, Franzke CLE. Scale-dependency of the global mean surface temperature trend and its implication for the recent hiatus of global warming. Sci Rep. 2015;5:12971.
42. Gallegati M. A systematic wavelet-based exploratory analysis of climatic variables. Clim Change. 2018;148(1–2):325–38. https://doi.org/10.1007/s10584-018-2172-8
43. Kumar P, Foufoula-Georgiou E. Wavelet analysis for geophysical applications. Rev Geophys. 1997;35(4):385–412. https://doi.org/10.1029/97rg00427
44. Liu Y, Liang XS, Weisberg RH. Rectification of the bias in the wavelet power spectrum. J Atmos Ocean Technol. 2007;24:2093–102.
45. Schulte JA. Cumulative areawise testing in wavelet analysis and its application to geophysical time series. Nonlinear Process Geophys. 2016;23:45–57.
46. Grinsted A, Moore JC, Jevrejeva S. Application of the cross wavelet transform and wavelet coherence to geophysical time series. Nonlin Process Geophys. 2004;11(5/6):561–6. https://doi.org/10.5194/npg-11-561-2004
47. Schulte JA, Duffy C, Najjar RG. Geometric and topological approaches to significance testing in wavelet analysis. Nonlin Process Geophys. 2015;22(2):139–56. https://doi.org/10.5194/npg-22-139-2015
48. Fu C, Diaz HF, Fletcher JO. Characteristics of the response of sea surface temperature in the central Pacific associated with warm episodes of the Southern Oscillation. Mon Weather Rev. 1986;114:1716–38.
49. Trenberth KE, Stepaniak DP. Indices of El Niño evolution. J Clim. 2001;14:1697–701.
50. Atems B, Sardar N. Exploring asymmetries in the effects of El Niño-Southern Oscillation on U.S. food and agricultural stock prices. Q Rev Econ Finance. 2021;81:1–14. https://doi.org/10.1016/j.qref.2021.04.013
51. Liu Y, Cai W, Lin X, Li Z, Zhang Y. Nonlinear El Niño impacts on the global economy under climate change. Nat Commun. 2023;14(1):5887. https://doi.org/10.1038/s41467-023-41551-9 PMID: 37735448
52. Hudgins L, Friehe C, Mayer M. Wavelet transforms and atmopsheric turbulence. Phys Rev Lett. 1993;71(20):3279–82. https://doi.org/10.1103/PhysRevLett.71.3279 PMID: 10054933
53. Priya P, Dommenget D, McGregor S. The dynamics of the El Niño–Southern Oscillation diversity in the recharge oscillator framework. Clim Dyn. 2024;62(6):1–21. https://doi.org/10.1007/s00382-024-07158-6
54. Cai X, Sakemoto R. El Niño and commodity prices: new findings from partial wavelet coherence analysis. Front Environ Sci. 2022;10:893879.
55. Chudik A, Pesaran MH. Theory and practice of gvar modelling. J Econ Surv. 2016;30(1):165–97. https://doi.org/10.1111/joes.12095
56. Dell M, Jones BF, Olken BA. What do we learn from the weather? The new climate-economy literature. J Econ Lit. 2014;52:740–98.
57. Angrist JD, Pischke JS. Mostly harmless econometrics: an empiricist's companion. Princeton: Princeton University Press; 2009.
58. Pesaran MH, Smith R. Macroeconometric modelling with a global perspective. Manch Sch. 2006;74:24–49.
59. Pesaran MH, Schuermann T, Weiner SM. Modeling regional interdependencies using a global error-correcting macroeconometric model. J Bus Econ Stat. 2004;22:129–62.
60. Chudik A, Pesaran MH. Infinite-dimensional VARs and factor models. J Econom. 2011;163:4–22.